I R A M P
11(1), Jan 2020, pp. 1-6

ISSN: 2229-39-44

Alternative Principle for Measuring GigaGauss Magnetic Fields during Relativistic Laser-plasma Interactions by Analyzing X-Ray Spectral Lineshapes

E. DALIMIER[1], E. OKS[2*], AND P. ANGELO[1]

[1]*LULI - UPMC Univ Paris 06: Sorbonne Universités ; CNRS, Ecole Polytechnique, CEA: Université Paris-Saclay - F-75252 Paris cedex 05, France*
[2]*Physics Department, 380 Duncan Drive, Auburn University, Auburn, AL 36849, USA*
*Corresponding author email: goks@physics.auburn.edu

ABSTRACT: During relativistic laser-plasma interactions, super-strong magnetic fields of the GigaGauss (GG) or even multi-GG range could develop at the surface of the relativistic critical density. We present a new principle for measuring such magnetic fields during relativistic laser-plasma interactions. The principle can be realized by analyzing the profile of any hydrogenic x-ray spectral line, including the Lyman lines. Our new principle is applicable to the situation where there is a shift of the mid-point between the pair (or pairs) of the L-dip-structures in the experimental profile. We describe the step-by-step algorithm for determining the presence of the magnetic field and its strength B without the detailed modelling of the entire experimental profile. The subsequent modelling would only make the determination of the magnetic field strength B slightly more accurate. Our results should open the alternative way for using the shape of the x-ray spectral lines in future experiments for measuring super-strong magnetic fields developing during relativistic laser-plasma interactions.

Keywords: GigaGauss magnetic field; relativistic laser-plasma interactions; Langmuir-wave-caused dips in X-ray line profiles; ion acoustic waves; parametric decay instability

1. INTRODUCTION

During relativistic laser-plasma interactions, super-strong magnetic fields of the GigaGauss (GG) or even multi-GG range could develop at the surface of the relativistic critical density – according to, e.g., review [1] (and references therein) and articles [2-10]. Equation (11) from paper [2] states that the maximum magnetic field B_{max} is related to the laser intensity I by the following formula:

$$B_{max}\,(\mathrm{G}) = 10^{-1}[I(\mathrm{W/cm^2})]^{1/2}. \tag{1}$$

As experiments are now performed at the laser intensities $I \sim 10^{21}\mathrm{W/cm^2}$, as, e.g., in paper [11], the maximum magnetic fields could be as high as $B_{max} \sim 3$ GG or higher.

The highest magnetic field measured in laser-plasma experiments so far was $B \sim 0.7$ GG [3] obtained via the polarization measurements (the Cotton-Mouton effect of an induced ellipticity) of high-order VUV laser harmonics generated at the incident irradiation intensity $I = 9\mathrm{x}10^{19}$ W/cm^2. In the previous experiment [4, 5], a smaller magnetic field (up to $B \sim 0.4$ GG) was measured at the incident irradiation intensity up to $I = 9\mathrm{x}10^{19}$ W/cm^2 – by using the self-generated harmonics of the laser frequency and the fact that the magnetized plasma is birefringent and/or optically active (depending on the propagation direction of the electromagnetic wave).

Recently a couple of spectroscopic methods were suggested for measuring GG magnetic fields arising during relativistic laser-plasma interactions. In paper [12] the authors proposed a method for measuring GG magnetic fields utilizing the phenomenon of Langmuir-wave-cased dips (L-dips, or more rigorously L-dip-structures) in x-ray line profiles. The L-dips were identified in x-ray spectral line profiles and used for diagnostics in several experimental

studies of relativistic laser-plasma interactions – see, e.g., articles [11, 13] and review [14]. The idea behind paper [12] was that the separation of the L-dips from one another can be used to measure super-strong magnetic fields because they affect this separation.

In paper [15] the authors suggested measuring super-strong magnetic fields by employing the other effect of such fields on the L-dips: the dependence of the halfwidth of the L-dips on these fields. In distinction to the method from paper [12], which was not applicable to the Lyman lines, the method from paper [15] was applicable to the lines of any spectral series, including the Lyman lines. This was practically important: the x-ray Lyman lines are most frequently and most easily observed in laser-plasma interaction experiments.

In the present paper we describe a new principle for measuring super-strong magnetic fields during relativistic laser-plasma interactions. The principle can be realized by analyzing the profile of any hydrogenic x-ray spectral line, including the Lyman lines. The principle is based on the intra-Stark x-ray spectroscopy and we focus here on situations where there is a shift of the mid-point between the pairs of the experimental L-dips structures, as explained below.

2. BRIEF THEORY OF THE L-DIP-STRUCTURES IN PROFILES OF HYDROGENIC SPECTRAL LINES

The mechanism behind the L-dip phenomenon is a resonant coupling between the quasi-monochromatic electric field **E** of the Langmuir waves and the quasistatic electric field **F** provided by the Low-frequency Electrostatic Plasma Turbulence (LET) and/or the ion microfield in plasmas. It has a rich underlying physics: it is a nonlinear dynamic-resonance effect of essentially multifrequency nature although the dynamic electric field, producing the L-dip phenomenon, is quasi-monochromatic – see, e.g., book [16].

The L-dip-structures in profiles of hydrogenic spectral lines, caused by the L-dip phenomenon, were first discovered experimentally in 1977 in paper [17]. In the intervening 43 years, the L-dip-structures were studied experimentally by various groups working at different plasma sources – see, e.g., references from books [16, 18]. The latest experimental studies revealed the L-dip-structures (in hydrogenic line profiles) arising from relativistic laser-plasma interactions [11, 13, 14] – see Fig. 1. The theory of L-dips provided a diagnostic tool for very accurate measurements of the electron density N_e and for measuring the electric field amplitude E_0 of the Langmuir waves, as explained below.

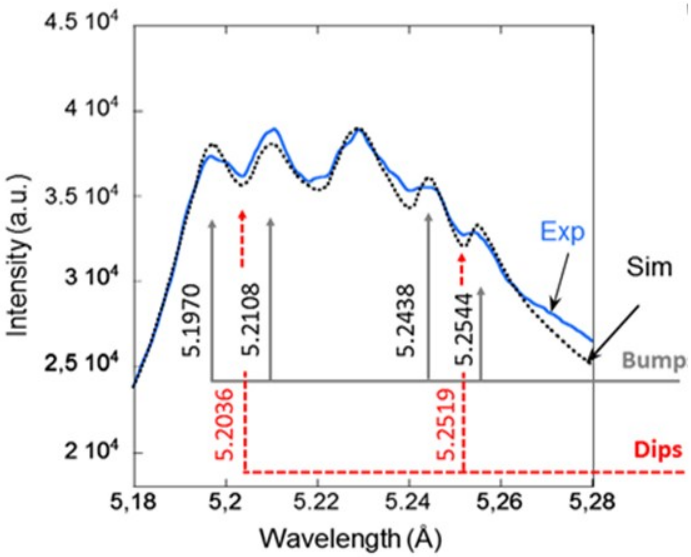

Fig. 1. Comparison of the experimental profiles of the Si XIV Ly-beta line (solid line, marked Exp) with the theoretical profiles (dotted line, marked Sim) [13]. The laser intensity was 2×10^{20} W/cm^2. There are clearly seen 'bump-dip-bump' structures (both in the red and blue parts of the profiles) typical for the L-dips phenomenon. The electron density deduced from the separation within the pair of the L-dips (one being in the red part and another – in the blue part of the profile) was $N_e = 2.2\times10^{22}$ cm^{-3},

In simple terms, the physics behind the L-dip-structures (according, e.g., to book [16]) is the following. A quasistatic electric field **F** in a plasma causes the Stark splitting of hydrogenic energy levels

$$\omega_{stark}(\mathrm{F}) = 3n\hbar\mathrm{F}/(2Z_r m_e e) \tag{2}$$

Here n is the principal quantum number, Z_r is the nuclear charge; m_e and e are the electron mass and charge, respectively. The field **F** differs for various radiating ions in the plasma: it has a distribution and so does the Stark splitting $\omega_{stark}(\mathrm{F})$. Therefore there is a group of radiating hydrogenic ions (hereafter, radiators), for which the Stark splitting is in resonance with the frequency ω_L of the Langmuir wave, the frequency ω_L practically coinciding with the plasma electron frequency $\omega_{pe} = (4\pi e^2 N_e/m_e)^{1/2}$:

$$\omega_{stark}(\mathrm{F}) = s\omega_{pe}(N_e), \quad s = 1, 2, \ldots \tag{3}$$

In Eqs. (2) and (3), n and Z_r are the principal quantum number and the nuclear charge of the radiator, s is the number of Langmuir plasmons (quanta) involved in the resonance.

The above resonance can manifest as L-dip-structures at certain locations (of hydrogenic line profiles) controlled by the electron density N_e. The L-dip-structures generally can consist of two local minima and two local maxima (bumps) in the line profile. The location of the primary minimum is controlled by the Langmuir wave frequency and thus by the electron density N_e. (Therefore, N_e can be determined from the separation between different such structures with a very high accuracy.) The near bump, i.e., the bump that is closer to the line center, being superimposed with the inclined line profile, can lead to the appearance of a secondary minimum or a small shoulder. If being superimposed on a sufficiently steep line profile, it is possible that the secondary minimum and even one or both bumps would not show up.

The theory of the L-dip-structures takes the simplest form when the states of the radiator are considered in the parabolic quantization: using in addition to the principal quantum number n also the electric quantum number $q = n_1 - n_2$ expressed through the parabolic quantum numbers n_1 and n_2: $q = 0, \pm1, \pm2, \ldots, \pm(n-1)$. It is convenient to label the Stark components of the Lyman lines by the electric quantum number q.

In the case where the quasistatic field **F** in the plasma is dominated by the LET, e.g., the ion acoustic turbulence, for each pair of Stark components, corresponding to the electric quantum numbers q and $-q$, there could be a pair of the L-dips located symmetrically in the red and blue parts of the spectral line profile

$$\Delta\lambda_{dip}(qs, N_e) = \pm\left[\lambda_0^2/(2\pi c)\right] qs\omega_{pe}(N_e). \tag{4}$$

It is seen that the location of the pair of L-dips is controlled by the product $|q|s$ for a given electron density N_e. Equation (4) gives the position of the primary local minimum of the intensity.

The quasistatic electric field required for the formation of the L-dips would be represented by the LET if it would be much stronger than the ion microfield. In this situation, there would be no shift of the mid-point between the two L-dips in the pair – as , e.g., in the experimental profile of the Ly-beta line of Si XIV (reproduced here as Fig. 1) from paper [13].

In the opposite scenario, e.g., if there would be no LET, then for electron densities $N_e > 10^{22}$ cm^{-3}, the mid-point between the two L-dips in the pair would be red-shifted due to the spatial non-uniformity of the ion microfield at the location of the radiating ions [16, 19]. This shift increases with N_e and for sub-solid-state densities could reach the several tens of mÅ. This situation, as well as the intermediate scenario (where the ion microfield and the LET have comparable strengths) could occur at laser intensities higher than 2×10^{20} W/cm^2.

3. TESTS REQUIRED FOR IDENTIFYING L-DIP-STRUCTURES IN EXPERIMENTAL LINE PROFILES

It should be emphatically underscored that in many cases, modulations in some experimental profile of a hydrogenic

line have nothing to do with the L-dip phenomenon. The process of establishing whether the modulations in some experimental profile of a hydrogenic spectral line are related to L-dip structures involves multiple tests of self-consistency, as follows.

Test #1. L-dip structures (if any) should appear both in the red and blue parts of the experimental profile and (in the 1st approximation) should be approximately symmetric with respect to the line center.

Test #2. The value of N_e, determined from the separation between these 2 structures (one in the red part, another in the blue part) should make sense physically at least by the order of magnitude. (This separation is controlled by the Langmuir wave frequency, which in its turn is controlled by N_e.)

Test #3. If there is more than one pair of such structures, then the values of N_e, determined from the separation within the two different pairs, should coincide.

Test #4. If there is a red shift of the mid-point within the pair of structures, then the values of N_e, determined from the mid-point-shift for two different structures, should coincide.

Test #5. The separation within the pair of such structures also determines the resonant value F_{res} of the quasistatic electric field (involved together with the Langmuir field in the production of the L-dip structure and determined by Eq. (3)). The halfwidth of the L-dip-structure determines the amplitude E_0 of the Langmuir field. Then the condition should be met: $E_0 < F/2$. Otherwise, according to the theory [16], no L-dip structures can be produced.

Test #6. All local minima and maxima in the experimental profile should be explained by L-dip structures – except for far wings dominated by the noise (Once again, one L-dip structure can explain up to two local minima and two local maxima of intensity.)

Only after all six of the above tests would be successfully passed, one can proceed with applying the new principle for measuring GG magnetic fields, as presented in the next section.

4. DESCRIPTION OF THE NEW PRINCIPLE

For explaining the new principle we use, as an example, the Ly-beta line of Si XIV – the line used, e.g., in the experiments analyzed in papers [11, 13]. We consider the situation where the modulations in the experimental profile of this line successfully passed all six tests (listed in Sect. 3) to qualify as the L-dip-structures.

From Eq. (4) follows an interesting characteristic feature of the Ly-beta line. Namely, the L-dip-structure in the profile of the component of $q = 1$ originating from the two-quantum resonance ($s = 2$) coincides by its location with the L-dip in the profile of the component of $q = 2$ originating from the one-quantum resonance ($s = 1$). As a result, the L-super-dip of a significantly higher visibility is formed.

So, the most pronounced would be the pair of the L-dip-structures corresponding to $|q|s = 2$: one L-super dip – in the blue part and the other L-super-dip in the red part. From the separation between the two L-super-dips, by using Eq. (4) one can deduce the electron density N_e. (It should be emphasized that this passive method for measuring N_e has the same high accuracy as the active spectroscopic method using the Thompson scattering, as shown in paper [19].)

As for the possible pair of the L-dips corresponding to $|q|s = 1$, it may or may not show up in the experimental profile. For example, the experimental Ly-beta profiles of Si XIV presented in paper [13] did not show this pair of the L-dips. Those profiles were obtained at the laser intensity in $2x10^{20}$ W/cm^2 and the electron density deduced from the experimental L-super-dips was $2.2x10^{22}$ cm^{-3}. However, at higher laser intensities and therefore higher electron densities, the pair of the L-dips corresponding to $|q|s = 1$ can be visible. This is because for higher electron densities, the location of possible L-dips, corresponding to $|q|s = 1$, would be further away from the line center compared to the experiments at Vulcan [13], where their possible location corresponded to the part of the line profile where the low-frequency field was not quasistatic (and thus no resonance and no L-dips).

Now we focus on the possible experimental shift of the mid-point between the pair (or pairs) of the L-dip-

structures. We remind that if there would be no LET, then the mid-point would be significantly red-shifted. For example, for the electron density $Ne = 5x10^{22}$ cm^{-3}, the mid-point would be red-shifted by 13.8 mA for the L-dips pair of $|q|s = 2$ and by 7.4 mA for the L-dips pair of $|q|s = 1$. In the opposite case, where the quasistatic electric field in the plasma would be dominated by the LET, there would be no shift of the mid-point between the pair (or pairs) of the L-dip-structures.

Our new principle for measuring super-strong magnetic fields during relativistic laser-plasma interactions is applicable to the situation where there is a shift of the mid-point between the pair (or pairs) of the L-dip-structures – though not necessarily equal to the maximum possible shift (which is the shift in the situation where there is no LET). Here is the succession of the logical steps.

1. From the experimental separation between a pair of the L-dip structures to determine the electron density N_e with a high accuracy. This enables also to calculate the characteristic strength of the ion microfield F_{ion}.
2. From the shift of the mid-point between the pair (or pairs) of the L-dip-structures, knowing the characteristic strength of the ion microfield (from step 1), to determine the characteristic strength F_{LET} of the LET (if any).
3. Knowing the F_{ion} and F_{LET} from steps 1 and 2, to calculate the Full Width at Half Maximum (FWHM) of the theoretical Stark profile, including also the broadening by plasma electrons: $\Delta\lambda_{1/2S}$. The temperature required for calculating the contribution by plasma electrons can be estimated as $T(eV) \sim 2.5Z^2$, where Z is the nuclear charge of the radiating ions. This estimate of T typically has the accuracy of about 20%. For the broadening by plasma electrons, which scales as $\sim 1/T^{1/2}$, formula $T(eV) \sim 2.5Z^2$ would therefore yield the accuracy of about 10%. This accuracy is sufficient especially because for the plasmas created by relativistic laser-plasma interactions, the broadening by plasma electrons is small compared to the broadening by the LET and/or the ion microfield.
4. For plasmas created during relativistic laser-plasma interactions, the Stark broadening of the hydrogenic x-ray spectral lines usually predominates over the Doppler broadening. However, the Doppler broadening can be added for calculating the FWHM of the Stark-Doppler theoretical profile $\Delta\lambda_{1/2SD}$ by using the estimate $T(eV) \sim 2.5Z^2$. Since Doppler broadening scales as $\sim T^{1/2}$, formula $T(eV) \sim 2.5Z^2$ would therefore yield the accuracy of about 10%. This accuracy is sufficient especially because for the plasmas created by relativistic laser-plasma interactions, the Doppler broadening is small compared to the broadening by the LET and/or the ion microfield.
5. If the FWHM of the theoretical profile $\Delta\lambda_{1/2SD}$ is noticeably smaller than the FWHM of the experimental profile $\Delta\lambda_{1/2exp}$, the next step would be to check whether the experimental profile is affected by some opacity. For the example of the Ly-beta line, if the top of the experimental profile exhibits the doublet structure (typical for the theoretical profiles of the Ly-beta line), then the optical depth at the top of the profile is $\tau_0 << 1$, so that the opacity cannot make a noticeable contribution to the FWHM of the experimental profile.
6. If in step 5 it would be established that $\tau_0 << 1$, then this would proof that the noticeable excess of the experimental FWHM $\Delta\lambda_{1/2exp}$ compared to the FWHM $\Delta\lambda_{1/2SD}$ of the theoretical Stark-Doppler profile is due to a magnetic field. The strength B of the magnetic field can be deduced from the difference $(\Delta\lambda_{1/2exp} - \Delta\lambda_{1/2SD})$ by using the standard formula for the Zeeman effect for hydrogenic spectral lines.

It is important to emphasize that the above algorithm allows determining the presence of the magnetic field and its strength B without the detailed modelling of the entire experimental profile. The subsequent modelling would only make the determination of the magnetic field strength B slightly more accurate.

5. CONCLUSIONS

We presented a new principle for measuring super-strong magnetic fields during relativistic laser-plasma interactions. The principle can be realized by analyzing the profile of any hydrogenic x-ray spectral line, including the Lyman lines.

Our new principle is applicable to the situation where there is a shift of the mid-point between the pair (or pairs) of the L-dip-structures in the experimental profile. We described the step-by-step algorithm for determining the presence of the magnetic field and its strength B without the detailed modelling of the entire experimental profile. The subsequent modelling would only make the determination of the magnetic field strength B slightly more accurate.

We believe that our results open up the way for using the shape of the x-ray spectral lines in future experiments for measuring super-strong magnetic fields developing during relativistic laser-plasma interactions.

References

1. V.S. Belyaev, V.P. Krainov, V.S. Lisitsa, A.P. Matafonov, Generation of fast charged particles and superstrong magnetic fields in the interaction of ultrashort high-intensity laser pulses with solid targets, Physics – Uspekhi 51 (2008) 793 - 814.
2. V.S. Belyaev, A.P. Matafonov, Fast charged particles and super-strong magnetic fields generated by intense laser target interaction, in: A. Andreev (Ed.), Femtosecond-Scale Optics, InTech, Shanghai, 2011, pp. 87 - 112.
3. U. Wagner, M. Tatarakis, A. Gopal et al, Laboratory measurements of 0.7 GG magnetic fields generated during high-intensity laser interactions with dense plasmas, Phys. Rev. E 70 (2004) e026401.
4. M. Tatarakis, A. Gopal, I. Watts et al, Measurements of ultrastrong magnetic fields during relativistic laser–plasma interactions, Phys. Plasmas 9 (2002) 2244 - 2250.
5. M. Tatarakis, I. Watts, F.N. Beg et al, Measuring huge magnetic fields, Nature 415 (2002) 280 - 280.
6. S. Kato, T. Nakamura, K. Mima, Y. Sentoku, H. Nagatomo, Y. Owadano, Generation of quasistatic magnetic field in the relativistic laser-plasma interactions, J. Plasma Fusion Res. SERIES 6 (2004) 658 - 661.
7. F. Perogaro, S.V. Bulanov, F. Califano et al, Magnetic fields from high-intensity laser pulses in plasmas, Plasma Phys. Control. Fusion 38 (1997) B261 – B272.
8. M. Singh, K. Gopal, D. Gupta, Temporally asymmetric laser pulse for magnetic-field generation in plasmas, Phys. Letters A 380 (2016) 1437 - 1441.
9. T.V. Liseykina, S.V. Popruzhenko, A. Macchi, Inverse Faraday effect driven by radiation friction, New Journal of Physics 18 (2016) e072001.
10. J.J. Santos, M. Bailly-Crandvaux, M. Ehret et al, Laser-driven strong magnetostatic fields with applications to charged beam transport and magnetized high energy-density physics, Physics of Plasmas 25 (2018) e056705.
11. E. Oks, E. Dalimier, A.Ya. Faenov et al, Using X-ray spectroscopy of relativistic laser plasma interaction to reveal parametric decay instabilities: a modeling tool for astrophysics, Optics Express **25** (2017) 1958 - 1972.
12. E. Dalimier, E. Oks, X-ray spectroscopy based diagnostic of GigaGauss magnetic fields during relativistic laser-plasma interactions, Atoms 6 (2018) 60.
13. E. Oks, E. Dalimier, A.Ya. Faenov et al, In-depth study of intra-Stark spectroscopy in the x-ray range in relativistic laser-plasma interactions, J. Phys. B: At. Mol. Opt. Phys. 50 (2017) e245006.
14. E. Dalimier, T. Pikuz, P. Angelo, Mini-review of Intra-Stark x-ray spectroscopy of relativistic laser–plasma interactions, Atoms 6 (2018) 45.
15. E. Oks, E. Dalimier, and P. Angelo, Spectrochimica Acta B **157** (2019) 1.
16. E. Oks, *Plasma Spectroscopy: The Influence of Microwave and Laser Fields*, Springer Series on Atoms and Plasmas, vol. 9 (Springer, New York) 1995.
17. A.I. Zhuzhunashvili and E.Oks, Sov. Phys. JETP **46** (1977) 1122.
18. E. Oks, *Diagnostics of Laboratory and Astrophysical Plasmas Using Spectral Lineshapes of One-, Two-, and Three-Electron Systems"* World Scientific, Singapore) 2017, Chapter 7.
19. E. Oks, St. Böddeker, and H.-J. Kunze, Phys. Rev. A **44** (1991) 8338.